Multiplexed Functional Assessment of Genetic Variants in *CARD11*

Iana Meitlis,[1,19] Eric J. Allenspach,[1,2,6,19] Bradly M. Bauman,[7] Isabelle Q. Phan,[1] Gina Dabbah,[7] Erica G. Schmitt,[8] Nathan D. Camp,[1] Troy R. Torgerson,[9] Deborah A. Nickerson,[1,3,6] Michael J. Bamshad,[2,3,6] David Hagin,[10] Christopher R. Luthers,[7] Jeffrey R. Stinson,[7] Jessica Gray,[11] Ingrid Lundgren,[12] Joseph A. Church,[13] Manish J. Butte,[14] Mike B. Jordan,[11] Seema S. Aceves,[15] Daniella M. Schwartz,[16] Joshua D. Milner,[17] Susan Schuval,[18] Suzanne Skoda-Smith,[1,2] Megan A. Cooper,[8] Lea M. Starita,[3,6] David J. Rawlings,[1,2,4] Andrew L. Snow,[7] and Richard G. James[1,2,5,6,*]

Summary

Genetic testing has increased the number of variants identified in disease genes, but the diagnostic utility is limited by lack of understanding variant function. *CARD11* encodes an adaptor protein that expresses dominant-negative and gain-of-function variants associated with distinct immunodeficiencies. Here, we used a "cloning-free" saturation genome editing approach in a diploid cell line to simultaneously score 2,542 variants for decreased or increased function in the region of *CARD11* associated with immunodeficiency. We also described an exon-skipping mechanism for CARD11 dominant-negative activity. The classification of reported clinical variants was sensitive (94.6%) and specific (88.9%), which rendered the data immediately useful for interpretation of seven coding and splicing variants implicated in immunodeficiency found in our clinic. This approach is generalizable for variant interpretation in many other clinically actionable genes, in any relevant cell type.

Introduction

Precision medicine requires accurate predictions for the effects of variants in genes known to be associated with disease. However, the vast majority (> 98%) of clinical variants are interpreted as variants of uncertain significance (VUSs), because their effect on the underlying function of the gene-product and therefore disease is unknown.[1,2] VUSs should not be used to guide treatment decisions,[3] so VUS results frequently lead to confusion and concern among treating physicians and patients, thereby limiting the clinical utility of genetic testing.

Dominant variants in the multi-adaptor immune signaling protein, CARD11 (MIM: 607210), are implicated in two rare primary immunodeficiency syndromes. Gain-of-function variants are associated with a lymphoproliferative disorder known as B cell expansion with NF-κB and T cell anergy (BENTA [MIM: 616452]), which can lead to lymphoma.[4] In contrast, variants with loss-of-function are associated with two distinct immune diseases: heterozygous dominant-negative variants are associated with combined immune deficiency, which also variably presents with atopy and other autoimmune features (IMD11B; also known as CARD11-associated atopy with dominant interference of NF-κB signaling [CADINS]; [MIM: 617638]),[5,6] while homozygous or compound heterozygous loss-of-function *CARD11* variants are associated with severe combined immunodeficiency (SCID) (IMD11A [MIM: 615206]).[7] Haploinsufficiency of CARD11 is not associated with disease.[8] Individuals with *CARD11*-associated disease harboring gain-of-function variants need regular evaluation of lymphoma risk, whereas those with dominant-negative variants require aggressive treatment of their autoimmune and atopic symptoms. Using sequence data alone, it is currently impossible to predict which variants in *CARD11* decrease or increase protein function.

[1]Seattle Children's Research Institute, Seattle, WA 98101, USA; [2]Department of Pediatrics, University of Washington, Seattle, WA 98195, USA; [3]Department of Genome Sciences, University of Washington, Seattle, WA 98195, USA; [4]Department of Immunology, University of Washington, Seattle, WA 98195, USA; [5]Department of Pharmacology, University of Washington, Seattle, WA 98195, USA; [6]Brotman-Baty Institute for Precision Medicine, Seattle, WA 98195, USA; [7]Department of Pharmacology & Molecular Therapeutics, Uniformed Services University of the Health Sciences, Bethesda, MD 20814, USA; [8]Department of Pediatrics, Division of Rheumatology/Immunology, Washington University in St. Louis, MO 63130, USA; [9]Allen Institute for Immunology, Seattle, WA 98109, USA; [10]Allergy and Clinical Immunology Unit, Department of Medicine, Tel Aviv Sourasky Medical Center and Sackler Faculty of Medicine, University of Tel Aviv, Tel Aviv 62919, Israel; [11]Divisions of Immunobiology, and Bone Marrow Transplantation and Immune Deficiency, Cincinnati Children's Hospital Medical Center, University of Cincinnati College of Medicine, Cincinnati, OH 45229, USA; [12]St. Luke's Children's Hospital, Boise, ID 83712, USA; [13]Department of Pediatrics, Keck School of Medicine, University of Southern California and Children's Hospital Los Angeles, Los Angeles, CA 90033, USA; [14]Division of Immunology, Allergy, and Rheumatology, Department of Pediatrics, University of California Los Angeles, Los Angeles, CA 90404, USA; [15]Division of Allergy Immunology, Departments of Pediatrics and Medicine, University of California, San Diego, and Rady Children's Hospital, San Diego, CA 92123, USA; [16]NIAID, National Institutes of Health, Bethesda, MD 20892, USA; [17]Department of Pediatrics, Columbia University Irving Medical Center, New York, NY 10032, USA; [18]Department of Pediatrics, Stonybrook University, Stony Brook, NY 11794, USA
[19]These authors contributed equally
*Correspondence: rickerj@u.washington.edu
https://doi.org/10.1016/j.ajhg.2020.10.015.

Multiplexed assays of variant effect[9] (MAVEs) have enabled simultaneous functional characterization of thousands of variants. Therefore, MAVEs can rapidly generate data that can be used as evidence for or against pathogenicity for genetic variants,[10,11] such as those found in *CARD11*. In a MAVE, all possible single-nucleotide or amino acid variants in a specific gene are subject *en masse* to a functional assay where the genotype is linked to phenotype such that DNA sequencing can be used to quantify the functional effect of each variant. MAVEs have been developed to measure the effects of variants in clinically relevant coding and non-coding sequences based on molecular function,[12–14] gene expression,[15,16] protein abundance,[14,16] and cellular viability.[17–19] One limitation of MAVEs is that human genes of interest are often overexpressed or assayed in non-human contexts.[12] Saturation genome editing (SGE),[17,20] which uses CRISPR-Cas9 to install genetic variants directly into the genomic copy of the gene, can alleviate problems associated with overexpression of cDNAs. However, SGE has previously been used effectively in a haploid cell line, HAP1, which is not useful for assessing dominant effects or those specific to B or T cell biology.

Here, we developed a cloning-free, SGE approach to functionally classify *CARD11* variants in a diploid human immune cell model. We generated functional scores for 2,542 coding and 38 noncoding variants of *CARD11*. We were also able to identify putative dominant-negative variants that cause exon skipping, which we also found in two unrelated families with *CADINS* disease. These results demonstrate that SGE in diploid cells is a powerful tool to assess variant function, including functional effects caused by non-coding variants. Finally, by combining functional data with clinical features, we classified seven *CARD11* variants recently found in our clinics as "likely pathogenic" for CADINS disease and posit that the data generated by this SGE can be used to interpret future clinical variants.

Material and Methods

Saturation Genome Editing

All CRISPR gRNAs (Table S7) targeting the CARD domain (amino acids 4–146) were designed using the Broad Institute's single gRNA design tool[21] and synthesized by Integrated DNA Technologies (IDT) as described previously.[22] Single-stranded ODN repair templates (Table S7) were ordered from IDT with asymmetrical homology arms (longer on the PAM-proximal side), complementary to the non-target strand of Cas9, and two phosphorothioate bonds on each end.[23]

Exons 3–5 of CARD11 were divided into 9 regions to be targeted with a single gRNA (sgRNA). For each sgRNA, libraries of ssODNs for each amino acid position were ordered from IDT with mixed bases NNK (N = A, C, G, or T; K = G or T), or NNM for non target strands (M = A or C) to generate HDR templates with each of the 20 possible amino acids and one of the STOP codons. Each ssODN introduced (1) two synonymous substitutions at and near the PAM site to prevent Cas9-mediated cleavage of repaired DNA and (2) a single NNK/NNM amino acid variant. For each region, 2×10^6 hu-

man TMD8 cells were electroporated as described previously[22] with 2.5 μM Cas9-gRNA complex (2.1:1.2 ratio) and 100 pmol of ssODNs (equimolar mix of oligonucleotides), and after electroporation cultured at 37°C in Iscove's modified Dulbecco's medium (IMDM) (Thermo Fisher Scientific) supplemented with 10% FBS and 55 mM beta-mercaptoethanol. Two days after transfection, a portion of the cells were lysed and their genomic DNA (gDNA) and mRNA isolated using Quick DNA Kit (Zymo Research) or AllPrep DNA/RNA Micro Kit (QIAGEN). The remainder of the cells were cultured in either IMDM with 50 nM Ibrutinib or IMDM with vehicle (DMSO). On day 16 post transfection, gDNA from the cells was harvested again.

Amplicon Sequencing

To avoid amplifying residual editing templates, each sample was amplified for 18 cycles with primers (Table S7) that generated 700–980 bp amplicons using GXL PrimSTAR Polymerase (TaKaRa). Samples were then purified with Agencourt AMPure XP reagent (Beckman Coulter) at 0.8 × beads to sample volume ratio according to manufacturer's protocol and amplified for another 7 cycles with locus-specific primers containing Illumina adaptor sequences. The amplicons were purified with 1 × AMPure beads and reamplified for 7 cycles using primers containing Illumina p5 and p7 sequences and a unique sample index. The amplicon library was verified for purity by PAGE gel, quantified by Qubit 3 (Thermo Fisher Scientific), pooled, and paired-end sequenced on an Illumina NextSeq with a NextSeq v2 300 cycle kit (Illumina). The amplicon sequencing results from this study have been deposited on the Gene Expression Omnibus, record number GEO: GSE152129.

Data Analysis, Scoring, and Classification of CARD11 Variants

After Illumina sequencing, individual replicates (n = 5 per region) were de-multiplexed. Next, the data were filtered to isolate HDR events. We then used the Enrich2[24] algorithm and custom Python scripts to count variants and filter variants that were either poor quality, low coverage, or depleted at the RNA level. To generate functional scores for both assays, we scaled, normalized, and log transformed all variant count data. Finally, for the growth assay, individual variants were classified based on the distribution of the variant replicate data relative to that of all nonsense and synonymous variants. Variants were classified in the ibrutinib assay using the value for the lowest scoring known gain-of-function variant and the distribution of the synonymous variants. Detailed descriptions of the data analysis are found in the Supplemental Material and Methods.

Diagnosis and Genetic Sequencing

Clinical diagnosis was made by the referring immunologist. Whole-exome sequencing was performed in collaboration with University of Washington Center for Mendelian Genomics (UWCMG[25]), targeted clinical CARD11 Sanger sequencing (GeneDx), or clinical targeted panel (Invitae). Sanger sequencing also confirmed the variants. The procedures followed were in accordance with the ethical standards of the responsible committee on human experimentation (institutional and national) and proper informed consent was obtained.

NF-κB Reporter and Viability Assays

We measured NF-κB activity using three different methods. In OCI-Ly7 cells stably expressing a Gaussia NF-κB reporter, we introduced variants using gene editing as described above. Cells were

plated in a 96-well imaging microplate (Corning) at 40K cells per well (in replicates of 3) and cultured overnight in 100 μL of IMDM media supplemented with either vehicle (DMSO) or 33 nM Phorbol 12-myristate 13-acetate (PMA) and 1.4 mM ionomycin. After 16 h, NF-κB activity was quantified using a BioLux Gaussia Luciferase Assay Kit and cell viability read out using Cell-Titer-Glo Assay (Promega).

To study the downstream effects of intronic splicing variants and binding domain variants in CARD11 on NF-κB activity, we generated a CARD11-deficient Jurkat cell line by single cell dilution from cells transfected with a sgRNA targeting exon 3 of the CARD11 locus (guide ID 3.4). MND-wtCARD11-T2A-GFP vector was modified using overlapping oligonucleotides and restriction digest with Xho1 and BamHI to introduce point mutations or CARD11 exon-deficient variants. The cloning oligos are listed inTable S6 2×10^6 human CARD11-deficient Jurkat cells were simultaneously electroporated (Neon apparatus settings: 1,700V, 20 ms, 1 pulse) with 1,900 ng NF-κB-firefly luciferase reporter and 500 ng or 1,100 ng CARD11 vector. After resting in culture for 7 h, cells were plated in a 96-well imaging microplate at 100K cells per well in either RPMI culture media supplemented with vehicle (DMSO) or 33 nM PMA and 1.4 mM ionomycin. After 16 h of stimulation, NF-κB activation was measured as described above.

JPM50.6 and Jurkat CARD11 KO transfection experiments were used to assess dominant-negative activity in amino acid variants in CARD11 as previously described.[6] Briefly, 3×10^6 JPM50.6 cells were transfected with 3 μg of empty vector, WT or mutant pUNO-CARD11-FLAG plasmids in RPMI + 10%FCS using a BTX electroporator (Harvard Apparatus, 260V, 950 μF). Mutant CARD11 expression plasmids were produced via site-directed mutagenesis as previously described.[6] 24 h post-transfection, cells were stimulated with 1 μg/mL each of anti-CD3/CD28 antibodies (BD Biosciences) and cultured another 24 h. Relative NF-κB activity (based on κB-driven GFP mean fluorescence intensity) was quantified using an Accuri C6 flow cytometer (BD Biosciences).

To confirm protein expression, lysates were separated by SDS-PAGE, transferred to nitrocellulose, and blotted as previously described,[6] using the following antibodies: anti-CARD11 (clone 1D12) and anti-V5 (D3H8Q) (Cell Signaling Technologies), anti-FLAG (M2), and anti-beta-actin (AC-15) (Millipore Sigma). Blots were imaged and quantified using a LiCOR Odyssey system.

Modeling the CARD11 CARD Domain
The cryoEM map EMD-0013 was segmented with Segger and volumes corrected in Chimera using the BCL10-MALT1 fitted coordinates (PDB: 6GK2) as templates to obtain one segment per molecule.[26,27] CARD11 was remodelled on the BCL10 moiety of PDB: 6GK2 with Modeler.[28] Remodelled CARD11 structures were fitted into individual BCL10 segments of the cryoEM map with Segger. Experimentally observed high B-factor values at residues 64–66 in free CARD11 indicate that K69 is located in the vicinity of a highly dynamic loop, which is extended in free CARD11 and prevents the formation of a type III interface with BCL10. Remodeling CARD11 using UCSF Chimera with BCL10 (PDB: 6GK2), we assumed a conformation similar to polymerized BCL10 at the type III interface. This conformation placed K69 in a favorable electrostatic position for interaction with BCL10 E53. We also observed that K41, K69, and R72 in the remodeled CARD11 were in favorable positions to interact with the negatively charged residues of BCL10 at the type II interface.

Results

An Assay to Measure the Effect of CARD11 Variants on Function
CARD11, a 1,154 amino acid protein with seven functional domains, is required for B cell receptor-mediated activation of NF-κB[29] (Figure 1A). Growth of a human B cell lymphoma cell line, TMD8, is dependent on B cell receptor signaling (Figure 1B), CARD11 (Figure S1A), and NF-κB.[30] Therefore, we hypothesized that we could assess the functional effect of variants in CARD11 by measuring changes in cell growth. Additionally, the BTK inhibitor ibrutinib blocks B cell receptor signaling upstream of CARD11 and kills TMD8 cells (Figure S1B). However, since CARD11 promotes NF-κB signaling downstream of B cell receptor triggered BTK, gain-of-function CARD11 variants can rescue TMD8 survival (Figures S1C and S1D) in the presence of ibrutinib.[31]

Because decreased expression and alternative splicing are possible pathogenic mechanisms in CARD11-related disease, we introduced variants into the endogenous CARD11 locus by SGE. SGE has previously been performed in cultured human HAP1 cells, which have a haploid genome, a feature that simplifies analysis of loss-of-function variants. SGE in HAP1 also required transient transfection of Cas9 and repair templates on plasmids. In contrast, the TMD8 B cell line has a diploid genome but dies in response to transfection with plasmid DNA. To circumvent plasmid toxicity, we introduced Cas9 and guide RNAs as ribonucleoproteins along with libraries of single-stranded oligonucleotide (ssODN) repair templates[22,23] (Figure 1A). The repair templates contained synonymous variants that prevent Cas9 recutting and mixed bases (NNK) to introduce all possible amino acid substitutions into exons and single nucleotide variants at exon-intron junctions. We targeted exons 3–5, which encode the CARD, LATCH, and N-terminal coiled-coil domains (amino acids 4–146), where the majority of pathogenic germline CARD11 variants have been reported[32] (Figure 1A).

Assessing SGE in Diploid Immune Cells
To determine the feasibility of SGE in the TMD8 cell line, we assessed the homology-directed repair (HDR) rates for each single guide RNA (sgRNA) and repair template library by targeted sequencing. Total HDR ranged from 20% to 40% (Figure 1C). We determined the relative HDR rate at each nucleotide position by comparing the frequency of variant introduction at each position divided by the total HDR observed with each sgRNA. HDR efficiency directly correlated with proximity to the sgRNA target sites, with rates dropping substantially 10 bases 3′ to the cut site and 20 bases 5′ (Figures S2A–S2C). This result is consistent with reports showing HDR of double-strand breaks with ssODN repair templates is primarily accomplished using synthesis-dependent strand annealing, with conversion primarily occurring in an asymmetric distribution within
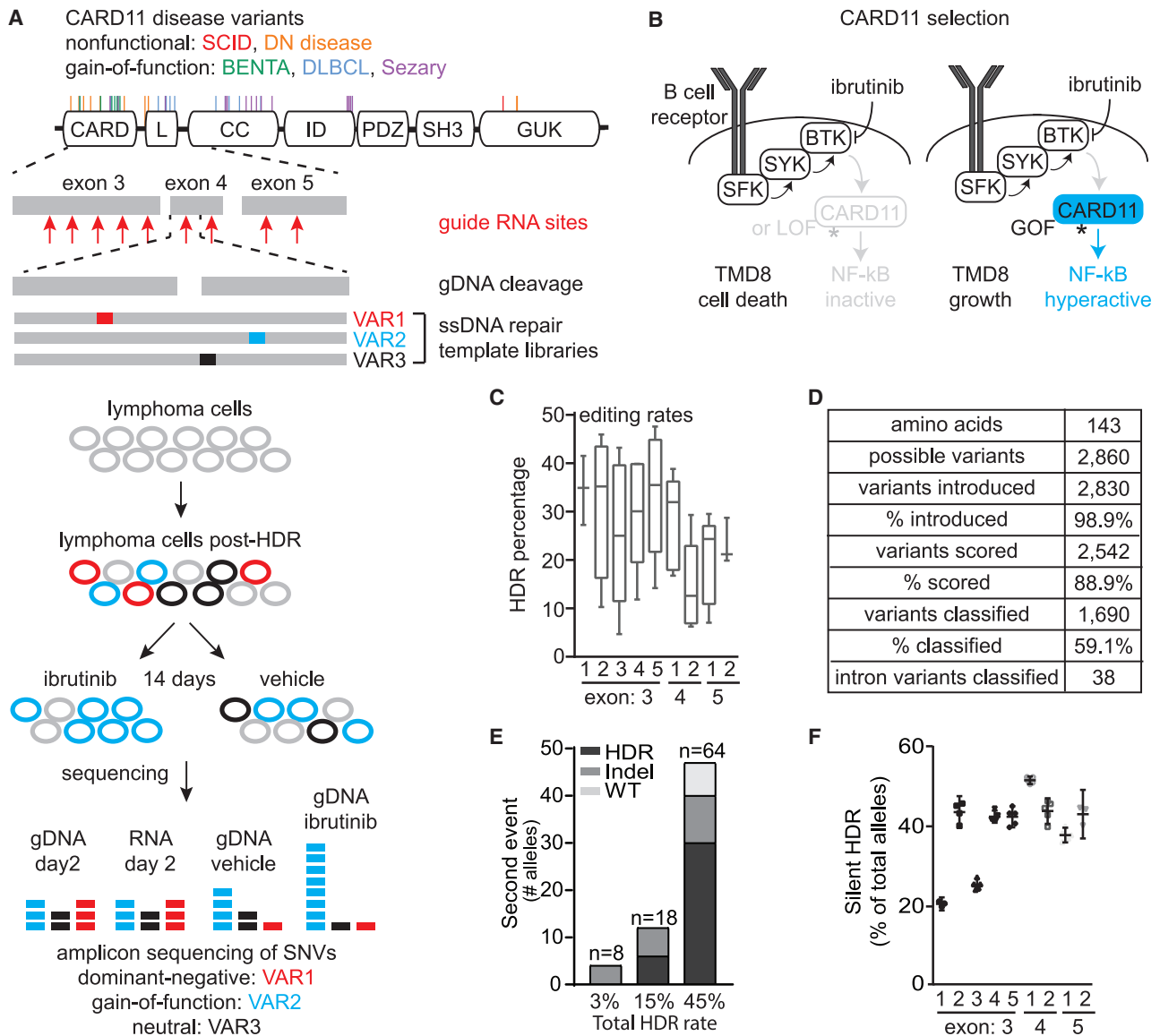
Figure 1. A Saturation Genome Editing Screen for Functional Assessment of *CARD11*

(A) A schematic of *CARD11* containing domains and sites of clinically documented mutations (red, severe combined immunodeficiency [SCID]; orange, CARD11-associated atopy with dominant interference of NF-κB signaling [CADINS]; green, B cell expansion with NF-κB and T cell anergy [BENTA]; blue, diffuse large B cell lymphoma [DLBCL]; and purple, Sezary).

(B) A schematic of B cell receptor signaling in TMD8 cells. Loss of *CARD11* or BTK inhibition with ibrutinib leads to TMD8 cell death. Gain-of-function mutations in CARD11 lead to constitutive activation of NF-κB, allowing TMD8 cells to survive in the presence of ibrutinib.

(C) HDR was used to introduce all possible amino acid variants into exons 3–5, including the CARD domain, where many variants associated with disease are located have been identified. gDNA from TMD8 lymphoma cells were sequenced 2 days after editing. A graph representing HDR rates for all replicates across each editing region plotted as a boxplot centered on the median with the whiskers representing the 5th-95th percentiles.

(D) Table summarizing the number of variants introduced, scored, and classified in the SGE experiment.

(E) TMD8 cells were edited at the CCR5 locus with increasing amounts of single-stranded oligonucleotide repair template to compare low, mid, and high editing rates. Monoclonal lines were isolated, and the identity of the other allele was quantified for cells containing at least one HDR allele.

(F) Quantification of the percentage of HDR events that solely introduce silent Cas9-blocking variants, which is plotted as mean ± standard error.

20 nt of the cut site.[33] The five replicate experiments were reproducible (pearson's R between 0.45 and 0.72) (Figure S3). We successfully introduced 98.9% of intended amino acid variants (Figure 1D), demonstrating the capacity of this SGE method for comprehensive assessment of variants in this region of *CARD11*.

Because we performed SGE in a diploid instead of a haploid cell line, we assessed the editing outcomes on
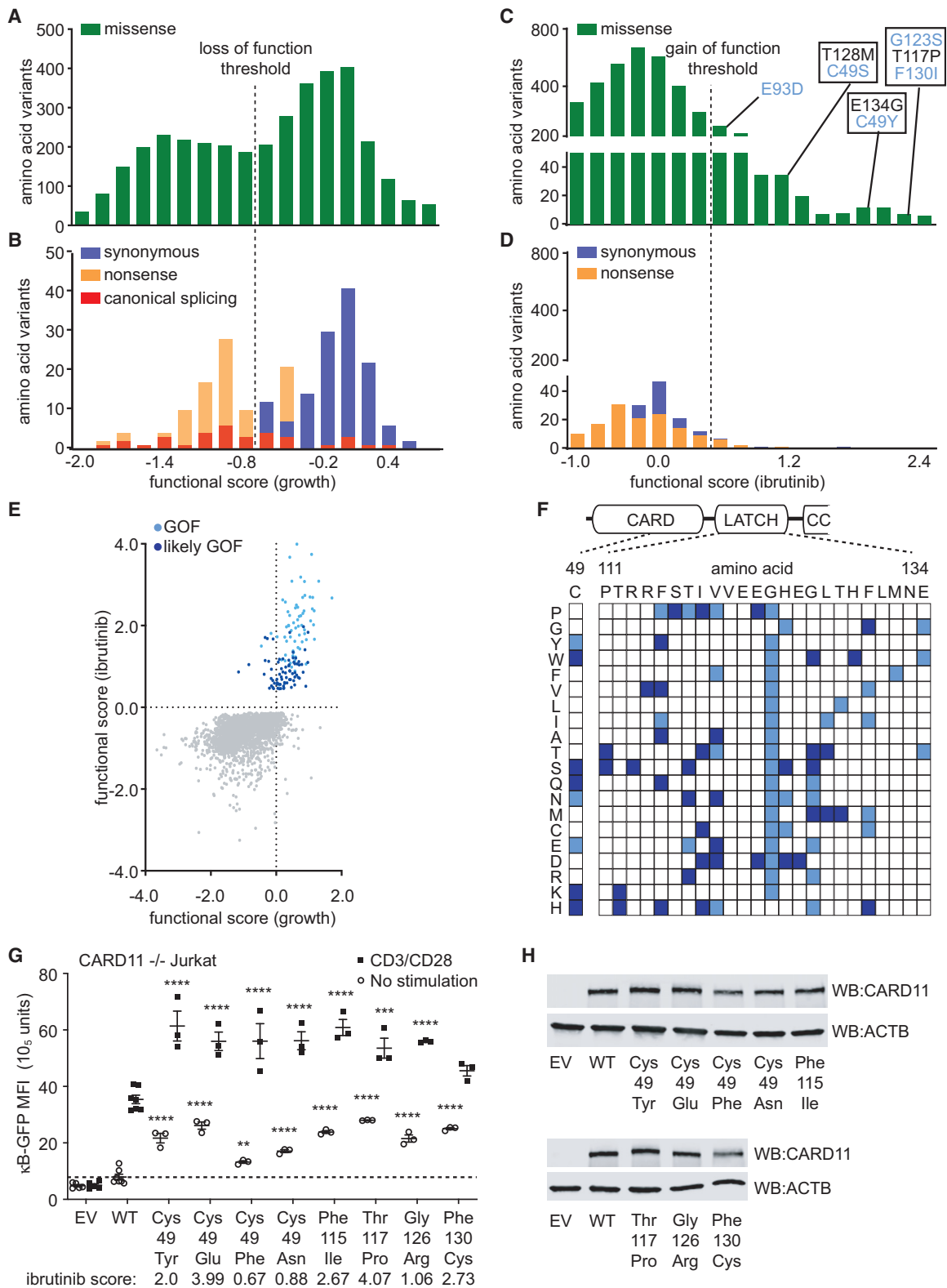
Figure 2. Pathogenic Gain-of-Function Variants in CARD11 Grow Selectively in the Presence of Ibrutinib

(A–D) Functional scores for all variants in the SGE experiment of *CARD11* using the cell growth and ibrutinib assays were plotted as distributions. The thresholds used to score loss-of-function (dotted line, A and B) and gain-of-function (dotted line, C and D) were indicated. The distribution of scores was plotted for all missense (A and C) and synonymous and nonsense variants (C and D). The location of activating variants in *CARD11* previously published to lead to BENTA were highlighted, or BENTA and DLBCL (light blue color) (C). (E) An X-Y scatterplot of functional scores from the growth (x axis) and ibrutinib (y axis) SGE. The functional classification of variants as gain-of-function or likely gain-of-function were annotated using the indicated colors.

both alleles in the same cell. To avoid complications due to selection, we introduced a variant into *CCR5*, which is not expressed in TMD8 cells and likely has no effect on viability. We varied HDR rates to mimic the observed rates we saw in the CARD11 SGE experiments, by introducing a sgRNA with increasing quantities of non-cleavable repair template to achieve low (3%), mid (15%), and high (45%) HDR. We analyzed 240 individual clonal cell lines to assess the editing outcomes at both alleles (HDR, NHEJ, unedited). At high HDR rates, like those observed in the SGE, we observed HDR events on both alleles in most cells that undergo HDR (Figure 1E).

Furthermore, in the SGE experiments, we found that almost half of quantified HDR events (Figure 1F) solely introduced the synonymous changes that prevent re-cleavage of repaired sequence by Cas9, and thus expressed wild-type protein. This likely occurred because the ssODN repair template libraries contained intended variants outside of the high-efficiency conversion zone for oligonucleotide-based HDR[33] (Figure S2). Taken together, the (1) high rates of bi-allelic HDR (Figure 1E) and (2) high rates of silent HDR in the SGE (Figure 1F) enable the identification of variants with decreased function, which include those that result solely in loss of protein function and those that also result in dominant-negative activity.

Identifying CARD11 Variants with Decreased or Increased Function

To determine the abundance of variants before outgrowth, genomic DNA (gDNA) was isolated from a portion of the cells 2 days after Cas9 transfection and variants were counted by targeted sequencing. We also sequenced cDNAs at this time point to identify variants depleted at the mRNA level. Then, to measure the effect of each variant on cell growth, cells were grown for an additional 14 days either without ibrutinib to assess variants that decrease function (growth assay) or with ibrutinib (ibrutinib assay) to assess variants that increase function. A functional score was computed for 88.9% of possible amino acid variants (Figures 2A–2D) and many intronic variants by taking the $\log_2$ ratio of the variant's count on day 14 divided by the count on day 2 and normalizing the result to the wild-type ratio (Tables S1, S2, and S3).

Since TMD8 cells require *CARD11* for survival and we observe some indel/HDR allele combinations (Figure 1E), we hypothesized that variants with decreased function would become depleted from the population during culture in medium without ibrutinib. We observed that the functional scores of nonsense and canonical splice variants

(orange and red bars, Figure 2B), which are predicted to decrease CARD11 function, are generally lower than those of synonymous variants (blue bars, Figure 2B). In contrast, the functional scores of missense amino acid variants were distributed bimodally (green bars, Figure 2A) with one peak overlapping the synonymous distribution and the other overlapping the distribution of the scores of nonsense variants. These data show that the growth assay differentiated functionally normal and loss-of-function missense variants in *CARD11*. We note that the separation of synonymous and nonsense variants is not mutually exclusive, likely because nonfunctional variants can be rescued by a functional allele of CARD11 on the other chromosome in diploid cells.

Ibrutinib Selection Identifies Variants that Increase CARD11 Function

Ibrutinib blocks NF-κB signaling via BTK inhibition and kills cultured TMD8 lymphoma cells; however, gain-of-function *CARD11* variants rescue cell growth by restoring NF-κB signaling downstream. Accordingly, ibrutinib treatment negatively skewed the distribution of functional scores for synonymous and most missense variants such that they directly overlapped with the distribution of nonsense variants scores (Figures 2C and 2D) leaving a small set of missense variants that were enriched. We hypothesized that these enriched variants might increase CARD11 function, and indeed measurements of the eight known gain-of-function variants[32,34] (e.g., p.Cys49Tyr, p.Gly123Ser, p.Gly123Asp, p.Glu134Gly) that are associated with BENTA were overrepresented in the ibrutinib-enriched set (Figure 2C; chi square $p = 2.4 \times 10^{-52}$; n = 5 replicates).

We classified variants that increase function as gain-of-function, likely gain-of-function, likely not gain-of-function, and not gain-of-function by their overlap with the synonymous or known gain-of-function distributions (Figures 2C and 2D). We then compared the functional scores of variants in the growth and ibrutinib assays and as predicted, the ibrutinib assay produced a much larger shift in previously validated gain-of-function variant functional scores than selection without drug (Figure 2E, Table S1). The majority of variants identified in the ibrutinib assay are located in two regions: at cysteine 49 and in the LATCH domain (amino acids 111–134; Figures 2F and S4), a domain critical for autoinhibition of CARD11 and CARD9.[34] 22 gain-of-function variants identified in a prior CARD11 overexpression screen,[34] as well as all known DLBCL variants that were scored in the ibrutinib assay,

(F) Gain-of-function variants were primarily clustered at cysteine 49, and in the N-terminal coiled-coil and the latch domains. Individual substitutions that promote gain-of-function activity are color coded as in (E).

(G) JPM50.6 cells were transfected with empty vector (EV), WT, or mutant CARD11 plasmids. NF-κB-driven GFP reporter expression ± 24 h anti-CD3/CD28 stimulation was quantified by flow cytometry and plotted as mean fluorescence intensity (MFI) ± standard error. Data are shown from three independent experiments; statistical significance versus WT (or WT+WT) was assessed using one-way ANOVA with the SIDAK correction for multiple comparisons ****$p < 0.0001$, **$p < 0.01$.

(H) Immunoblot showing CARD11-FLAG expression for each variant; ACTB serves as a loading control.

showed high concordance with the SGE functional scores (Figure S5A). To independently validate additional variants that increase CARD11 function, we assessed the effect of several using an NF-κB reporter assay. We introduced several variants classified as "gain-of-function" in our assay in the LATCH domain (p.Phe115Ile, p.Thr117Pro, p.Gly126Arg, and p.Phe130Cys) and at cysteine 49 (p.Cys49Tyr, p.Cys49Glu, p.Cys49Phe, and p.Cys49Asn) into JPM50.6 cells, a CARD11-deficient Jurkat T cell line that includes an integrated NF-κB-driven GFP reporter. We found that each variant significantly increased NF-κB reporter signal, either with or without stimulation by anti-CD3/CD28 antibodies (Figures 2G and 2H). Moreover, the degree of NF-κB activation in the absence of stimulation was highly correlated with functional scores in the ibrutinib assay (Figure S5B; Pearson's r = 0.9056). We also confirmed that several of the cysteine 49 variants increased NF-κB signaling in the Ly7 B cell line (Figure S5C). Finally, a variant at position (p.Gly123Val) was identified in a recently diagnosed BENTA-affected subject (Table S4). Using transient transfection of JPM50.6 cells, we found that p.Gly123Val CARD11 increased constitutive NF-κB activity (Supplemental Note, Table S4, Figures S5D–S5F). In summary, SGE results in the ibrutinib assay accurately predict gain-of-function effects on CARD11-dependent NF-κB signaling.

Classification of CARD11 Variants with Decreased Function

To classify variants found in the growth assay, we defined loss-of-function threshold as the upper bound of the 95% confidence interval for nonsense variants (dotted line, Figure 2A) and defined the functionally normal threshold as the lower bound of the confidence interval for synonymous variants (95%). We classified individual variants as functionally normal (n = 366) or likely functionally normal (n = 760) if the mean variant score was greater than the functionally normal threshold. If the lower bound of the confidence interval for the variant was not greater than the functional threshold, we classified the variant as likely functional. Conversely, we classified variants as nonfunctional (n = 668) or likely nonfunctional (n = 634) if the mean score was less than the nonfunctional threshold; likely nonfunctional was used when the upper bound of the confidence interval was greater than the nonfunctional threshold. Finally, all variants with confidence intervals that span or fall between the functional and nonfunctional thresholds were classified as "not definitive" (Table S2).

Functional Scores Accurately Predict CARD11 Dominant-Negative Activity in Variants Associated with CADINS Disease

We next investigated the relationship between the functional classification of CARD11 variants and RNA abundance. As expected, nonsense variants were depleted at the RNA level, most likely by nonsense-mediated decay (Table S3). Correlations between variant effect on RNA abundance and functional scores in the growth assay (Figure 3A) highlighted the expected result that nonsense and splicing variants were depleted in both assays (Pearson R = 0.54).

We also found many other missense variants that inhibited growth (Figure S6) in culture but were not depleted at the RNA level. Using a computational predictor of variant function, CADD,[35] we found that variants classified as nonfunctional or likely nonfunctional exhibited relatively high CADD scores (Figure 3B). However, variants that were classified as functional or likely functional exhibited a wide distribution of CADD scores that overlap with variants classified as nonfunctional, indicating that CADD scoring is sensitive to nonfunctional variants in CARD11, but is not highly specific.[36] Finally, we noted that many CARD11 variants classified as nonfunctional appeared to inhibit growth to a greater degree than nonsense variants (Figure 3A). Because this SGE enabled expression of variants in the presence of wild-type CARD11, we reasoned that a subset of low scoring variants might exhibit dominant-negative activity. Given this possibility, we tested whether the growth assay could sensitively classify known variants found in individuals with CADINS disease.

CADINS disease is a rare but likely underdiagnosed disorder, with 14 dominant-negative variants previously reported, 8 of which are in the CARD and LATCH domains of CARD11[5,6,37] (Figure 1A). Each of the 8 previously identified dominant-negative variants were scored as either nonfunctional or likely nonfunctional (Table S2, Figure S6) using the growth assay. During the course of this project, we identified five additional variants in the CARD domain from ten individuals with clinical phenotypes suggestive of CADINS disease. Each of these were also scored as nonfunctional or likely nonfunctional scores in the growth assay, which indicates decreased protein function (Table S2; p.Thr43Met, p.Asp58Gly, p.Val60Glu, p.Pro64Arg, and p.Arg72Leu).

To test whether these identified variants are dominant negative, we again used the gold-standard JPM50.6 NF-κB reporter assay.[6] Full-length CARD11 expressing each variant was transfected into CARD11-deficient JPM50.6 T cells. After activation with soluble anti-CD3 and -CD28, we quantified mean fluorescence intensity of NF-κB-driven GFP. Cells transfected with each of these variants exhibited significantly reduced NF-κB activity (Figure 3C), relative to controls. We next repeated the assay in the presence of co-transfected wild-type CARD11. Each of these variants potently inhibited CARD11-dependent NF-κB signaling (Figure 3D), indicating dominant-negative activity with comparable expression relative to wild-type protein (Figure 3E). After considering the associated clinical findings (Table S4 and Supplemental Note) and applying the American Society of Medical Genetics criteria for classification of variants, we concluded that each of these identified variants is
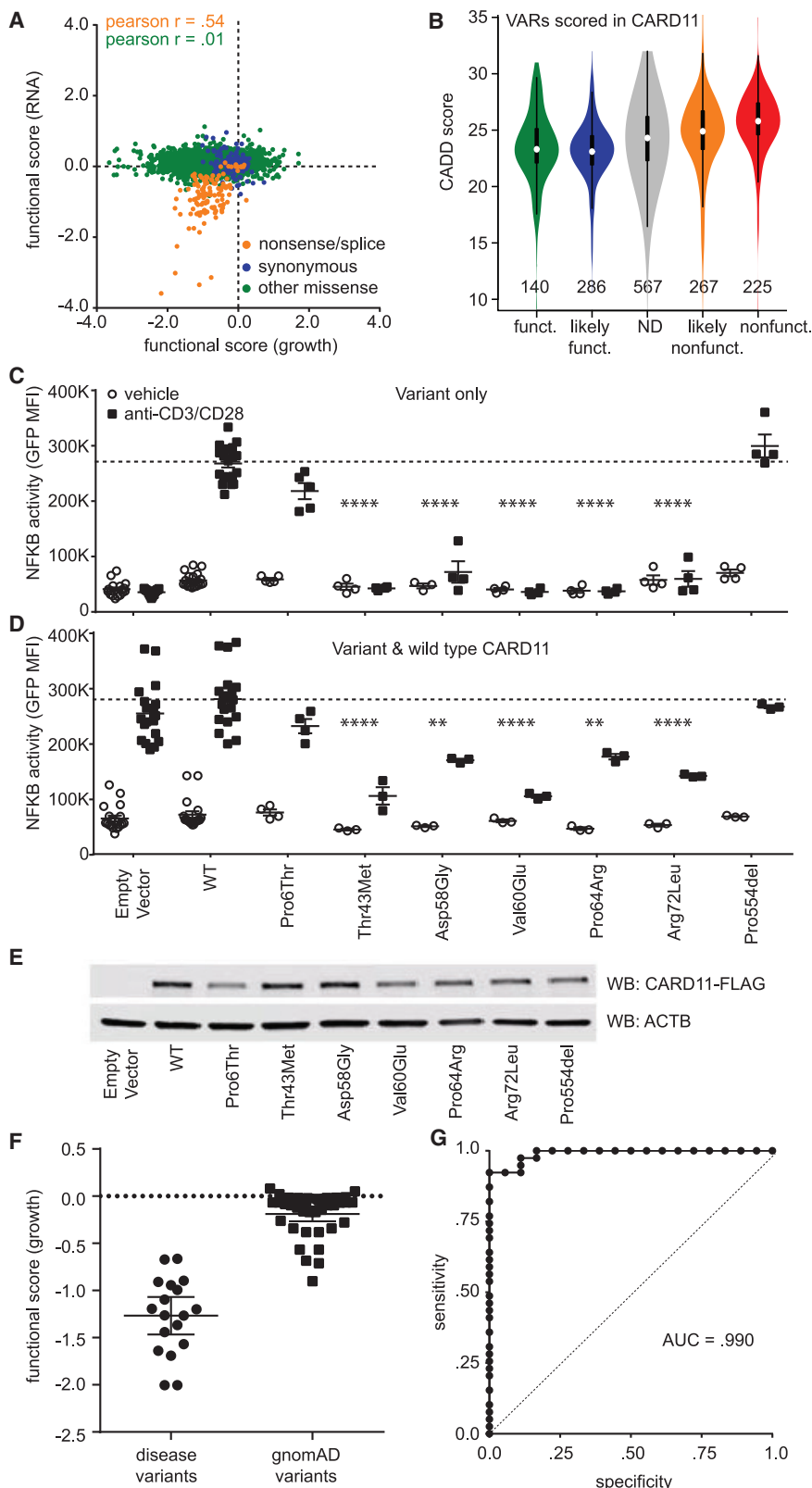
Figure 3. Functional Scoring from SGE Accurately Identify Variants that Decrease CARD11 Function

(A) An X-Y scatterplot showing SGE functional scores from RNA (y axis) versus the growth assay (x axis). Correlation scores between the variant effect on RNA abundance and growth were quantified (pearson) for nonsense/splice (orange) and all missense (green) variants.

(B) Violin plots showing the distribution of CADD scores for single nucleotide variants in each functional classification.

(C and D) JPM50.6 cells were transfected with empty vector (EV), WT or mutant CARD11 plasmids alone (C) or in 50:50 ratio with WT (D). After stimulation with anti-CD3/CD28, NF-κB-driven GFP reporter expression was quantified by flow cytometry and plotted as mean ± standard error. NS, non-stimulated. Statistical significance versus WT (or WT+WT) was assessed using one-way ANOVA with the SIDAK correction for multiple comparisons ****p < 0.0001, **p < 0.01.

(E) Immunoblot showing CARD11-FLAG expression for each variant; actin serves as a loading control.

(F) SGE functional scores were plotted for likely pathogenic/pathogenic variants and likely non-damaging variants present in gnomAD at a frequency greater than 1 in 300,000.

(G) A ROC curve reveals the sensitivity and specificity of SGE functional scoring for identification of these disease variants.

To investigate whether the *CARD11* functional scoring using the growth assay accurately predicted pathogenicity in cases screened for *CARD11* dominant-negative variants, we defined "disease" variants as those previously published[5,6,37] or characterized here based upon the clinical features (Table S4) and "healthy" as those present in gnomAD with frequencies higher than one in 300,000, which is higher than the expected incidence of CADINS disease (Supplemental Note). All measurements of CADINS disease-associated variants fell below the functional threshold (−0.216; Figure 3F). At the threshold we used to score non-functional variants (−0.711), a ROC curve showed a sensitivity of 94.6% at 88.9% specificity for the SGE data to detect dominant-negative variants (Figure 3G). We conclude that this growth assay meets the criteria for a validated

pathogenic or likely pathogenic (Table S5). The probands are being treated for CADINS disease, and these interpretations and evidence have been submitted to ClinVar.
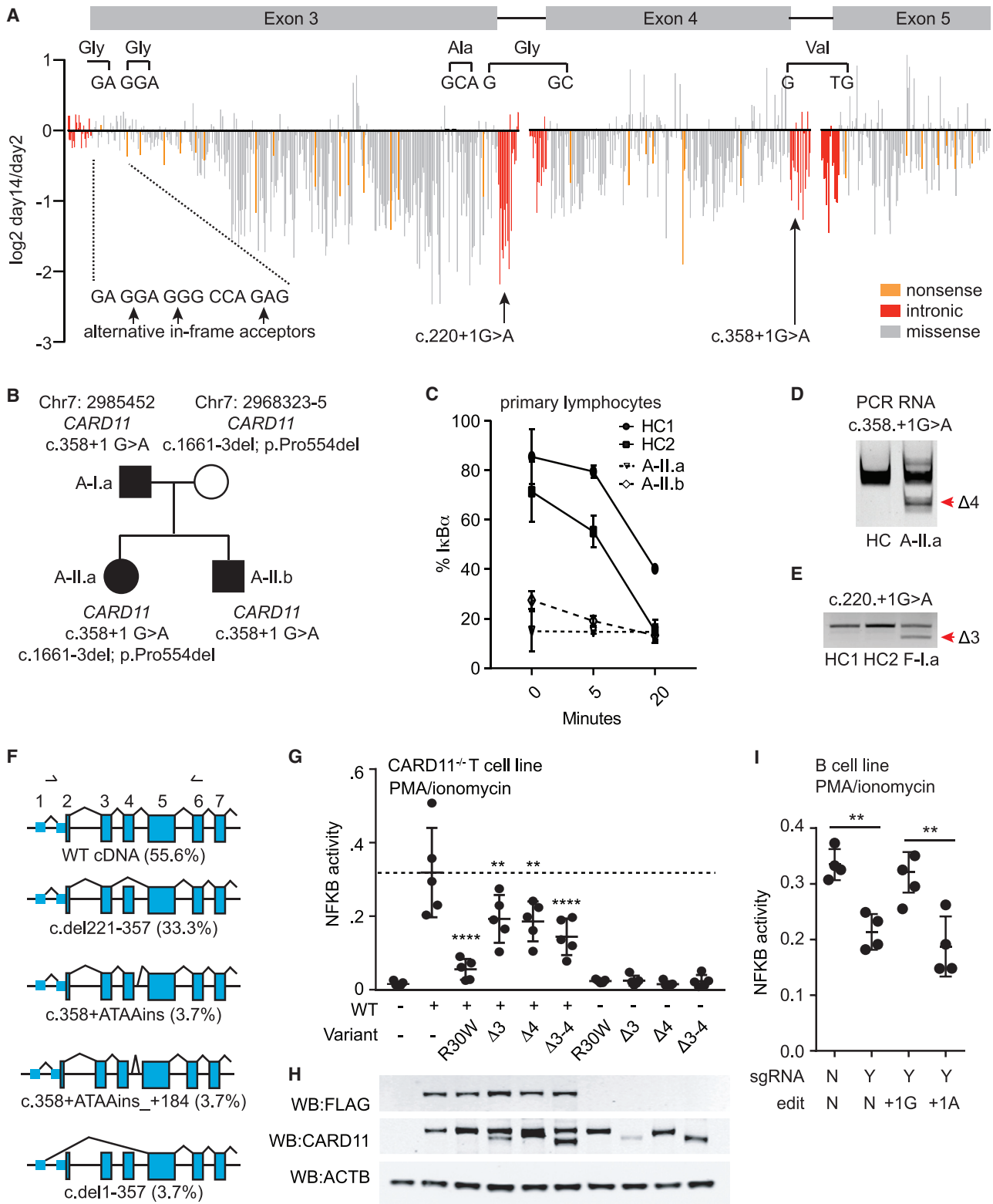
Figure 4. Splice Junction Variants Can Lead to Exon Skipping and Dominant-Negative Activity CARD11

(A) Functional scores for all single-nucleotide variants in the growth assay were plotted by position in each of the *CARD11* exons. Nonsense (orange) and intronic (red) variants were colored and exonic sequences spanning the intron-exon boundaries were labeled. Finally, we annotated the locations of two heterozygous variants identified in subjects with clinical suspicion for CARD11 dominant-negative disease.

(B) A pedigree chart shows inheritance of the c.358+1G>A variant in family A.

(C) PBMCs were isolated from healthy control subjects and case subjects (A-II.a and A-II.b) and stimulated with PMA for 0, 5, and 10 min. Ikb-alpha and phospho-ERK was quantified by flow cytometry and plotted as mean ± stardard deviation.

(legend continued on next page)

functional assay,[10] providing moderate evidence of pathogenicity for CADINS disease (> 11 likely pathogenic and > 11 likely benign variants used for assay validation) in the context of clinical suspicion.

Pathogenic In-Frame Exon Skipping in CARD11 Identified from Intronic Splicing Variants

Variants in the canonical splice acceptor and donor sequences often inhibited growth to a greater degree than nonsense variants (Figure 4A, red). A possible explanation for these findings is that variants in splice acceptors and donors in this region lead to expression of CARD11 that is missing all or part of one of the exons. Importantly, complete deletion of exon three, exon four, or both exons would produce an in-frame transcript (Figure 4A).

We identified two additional families with probands that exhibited clinical phenotypes consistent with CADINS disease with splice donor variants (hg38: chr7:2947574G>A; c.220+1G>A and hg38: chr7:2945818G>A; c.358+1G>A; Figures 4A and 4B and Supplemental Note). In one of these families, one of three affected individuals and her unaffected mother exhibited a second variant in CARD11 (p.Pro554del) not included in our screen, which had no functional effect using the NF-κB reporter assay (Figures 3C and 3D). Relative to healthy control subjects, white blood cells from two affected individuals (c.358+1G>A) exhibited decreased stimulation-induced NF-κB signaling and poor proliferative response to anti-CD3 stimulation (Figures 4B and 4C). We PCR amplified mRNA taken from white blood cells from affected individuals from both families and found additional high mobility bands with primers that flanked exon 4 (c.358+1G>A; Figure 4D) or exon 3 (c.220+1G>A; Figure 4E). Upon sequencing products from affected subjects with c.358+1G>A, we found that the smaller bands had a deletion of exon 4 (Figure 4F). These data confirm that individuals with these intronic variants in CARD11 express both full-length (from the wild type allele) and exon-deleted (from the c.358+1G>A or c.220+1G>A allele) RNA.

We next investigated whether in-frame deletions in the CARD domains of CARD11 (Δ exon 3, Δ exon 4, or Δ exon 3-4) alter NF-κB signaling. Using the NF-κB assay described above, we introduced each of these deletion constructs into CARD11-deficient T cells. None of the in-frame deletions in CARD11 were sufficient to promote NF-κB activity (Figure 4G). Additionally, each of these variants significantly inhibited wild-type CARD11 when co-transfected despite being expressed at lower abundance (Figure 4H), indicating that each exhibited dominant-negative activity. To further verify that the splice site change leads to altered NF-κB signaling, we used gene editing to introduce the c.358G>A variant into the Ly7 NF-κB reporter cell line. Unlike TMD8 cells, Ly7 cells do not require CARD11 for survival, but can respond to stimulus and activate NF-κB. After introducing the c.358G>A variant, or an adjacent silent mutation, we activated these cells with PMA/ionomycin and measured NF-κB activity. We found that cells receiving repair templates that introduce the silent variant, but not the c.358G>A, activate the NF-κB reporter (Figure 4I). Taken together, these data demonstrate that variants in CARD11 that lead to exclusion of either exons three, four, or both are likely to result in a dominant-negative form of CARD11. Consequently, individuals with clinical suspicion for CADINS disease that have splice variants in exons three through five in CARD11 should be evaluated for exon skipping, as these variants likely lead to dominant-negative activity rather than haploinsufficiency, which clinically has no known phenotype.

Functional Scores Imply that Disruption of the CARD11-BCL10 Interaction Leads to Dominant-Negative Activity

Data from gel filtration and structural modeling suggest that downstream signaling is initiated after CARD11 homo-trimerization, and then a CARD11-BCL10 interaction leads to formation of BCL10 filaments that scaffold downstream signaling proteins.[29,38,39] Crystal structures of the CARD11-BCL10 interface and alanine replacement experiments highlight the importance of four critical residues (Arg35, Lys41, Lys69, and Arg72) for CARD11-BCL10 co-immunoprecipitation and activation of NF-κB.[40] Functional scores from our growth assay similarly showed that positively charged residues in CARD11 known to be important for interaction between BCL10 and CARD11 (Arg35, Lys41, Lys69, and Arg72) are intolerant to most changes (Table S2), except conservative substitutions at Lys41, Lys69, and Arg72 that retain the positive charge. To further explore this interaction, we modeled the BCL10-CARD11 interaction by substituting CARD11 for one of the BCL10 proteins in the BCL10-BCL10 cryoEM structure (Figures 5A and 5B).[38] We found these positively charged residues to be in favorable positions to form

(D–F) cDNA was isolated from PBMCs of affected individuals with CARD11 splice variants (A-II.a and F-I.a) and amplified with the primers indicated on the exon-intron diagram in (F). These amplicons were analyzed via DNA PAGE gel (D and E) and colony sequencing (F).

(G) CARD11-deficient Jurkat cells were co-transfected with a plasmid expressing an NF-κB luciferase reporter and the indicated constructs. After stimulation with PMA/ionomycin, NF-κB reporter signal was quantified, normalized to cell viability, and plotted as mean ± standard deviation.

(H) Immunoblot showing CARD11-FLAG expression for each variant; actin serves as a loading control.

(I) Cas9 RNPs and HDR templates were used to introduce the indicated variants in place of c.358+1G in CARD11 into Ly7 lymphoma cells that express an NF-κB reporter. Following activation of CARD11-dependent signaling with PMA/ionomycin, reporter activity was normalized to cell viability, quantified, and plotted as mean ± starndard deveiation. For (G) and (I), we used one-way ANOVA with the SIDAK correction for multiple comparisons; ****$p < 0.0001$, **$p < 0.01$.

Figure 5. Modeling Conservative Changes to Amino Acid R35, K41, K69, and R72 of CARD11

(A and B) Structure of CARD11 protein CARD domain modeled based upon the cryoEM structures of BCL10 filaments in an (A) unbound state and (B) together with BCL10 illustrating the type III interaction. Blue indicates positive charge and red indicates negative charges.

(C and D) CARD11-deficient Jurkat cells were co-transfected with a plasmid expressing an NF-κB luciferase reporter and the indicated constructs. After stimulation with PMA/ionomycin, NF-κB reporter signal was quantified, normalized to cell viability, and plotted as mean ± standard deveiation. Variants highlighted in red have been previously identified in affected individuals. We used one-way AN-OVA with the SIDAK correction for multiple comparisons; ****p < 0.0001, **p < 0.01.

(E) Immunoblots showing CARD11 expression for each construct; actin serves as a loading control. Images are representative of two repeat experiments.

electrostatic interactions with BCL10 Glu53. We further tested the effects of selected changes using the NF-κB assay and found each replacement of the positively charged amino acid with either Leu or Gln rendered CARD11 to be nonfunctional (Figure 5C) and exhibit dominant-negative activity in an NF-κB assay (Figure 5D). In contrast, conservative changes at Lys41, Lys69, and Lys72 (p.Lys41Arg, p.Lys69Arg, p.Arg72Lys) that theoretically retained this electrostatic interaction behaved like wild type (Figures 5C and 5D). Consistent with these findings, a previously reported pathogenic variant p.Arg72Gly[6] and a pathogenic variant found in this study, p.Arg72Leu (Table S4), are associated with CADINS disease, which support the prior structural predictions and functional data.

Discussion

Here we describe an SGE approach to functionally characterize the effect of 2542 amino acid variants and 38 noncoding variants in their native genomic context in a critical region of CARD11. Features of our cloning-free SGE approach (high-efficiency RNP-ssODN co-delivery and synthesis-dependent annealing-based HDR) permitted introduction and analysis of variants in the presence of a wild-type copy of CARD11 expressed on the other allele. These key features of assay design enabled us to simultaneously identify variants that decrease or increase CARD11 function. The results of these two functional assays are highly accurate for predicting disease outcomes and add critical information, which we hope will aid diagnosis and treatment of individuals with suspected CARD11-associated disease (see Table S6 for a comprehensive summary of high-confidence functional variants). The simplicity of the approach will enable its use in a variety of cell types and possibly organisms, facilitating the tractability of MAVEs that query gene functions that are cell type specific, like that for CARD11.[41]

The American College of Medical Genetics and Genomics guidelines allows that functional evidence can be added to clinical evidence[3] to interpret genetic variants.[10] Clinical and molecular immunologists have historically regarded the NF-κB reporter assay as the gold-standard functional readout for dominant-negative and gain-of-function CARD11 variants.[4–6,37] With the Clingen guidelines for using functional assays as evidence for interpretation,[10] a positive result using the NF-κB reporter would solely provide "supporting" evidence for pathogenicity, primarily because there is scant published data showing the effect of known benign variants using the assay. We found that SGE functional scores predicted the effect of known likely pathogenic (>11) and likely benign (>11) variants in CADINS disease with high specificity (88.9%) and sensitivity (94.8%). Additionally, we independently validated the functional effects of several variants found in our screen using the NF-κB reporter assay. Based on the Clingen guidelines[10] and the number of known pathogenic and benign variants used to validate the ability of the assay to predict pathogenicity, the functional scores generated in the SGE growth assay should be used as "moderate" evidence for pathogenicity in patients with clinical suspicion for CADINS disease. Because we measured the effect of all variants in this region of CARD11, validation with additional known pathogenic or benign variants could increase the level of evidence to strong in the future.

The LATCH domain of CARD11 plays a crucial role mediating autoinhibition of the CARD and coiled-coil domains.[42] Structural data from the closely related CARD9 (MIM: 607212) shows that Gly111 (equivalent to Gly123 in CARD11) acts as a hinge between the LATCH and coiled-coil domains. The structural data suggested[39] that Gly111 is incompatible with any non-glycine residue, and its alteration is likely to disrupt the autoinhibitory interaction, leading to constitutive activation. Our data are also consistent with the structural data showing that other residues conserved between CARD9 and CARD11 are likely to be crucial for autoinhibition (including the following residues identified and validated in our screen as hotspots for gain-of-function variants: CARD11 Phe115, Thr117, Ile118, Val119, Gly126, and Leu127). After activation and release of auto-inhibition, the CARD domain functions as a nucleation factor for the CARD11-BCL10-MALT1 scaffold signaling complex.[38,42,43] The SGE results were consistent with biochemical data showing that Arg72, Lys69, Lys41, and Arg35 are collectively required for the interaction between the CARD domains of BCL10 and CARD11.[40] Our findings are consistent with the results from this report and show that replacement of each residue with nonpolar amino acids ablates NF-κB activity, even in the context of wild-type CARD11. Disruption of this interaction could partly explain the propensity of missense variants in the CARD domain to be associated with dominant-negative disease. We hope that the SGE functional scores will help improve our interpretation of CARD11 structural models.

We identified in-frame splicing defects that lead to exon exclusion within the CARD domain and expression of dominant-negative versions of CARD11. We predict that protein products lacking exons 3, 4, or both will behave similarly to CARD domain deletions, which fail to bind BCL10,[44] and this could explain their dominant-negative activity. The clinical importance of these findings became clear when we found two unrelated families with affected individuals presenting with phenotypes resembling CADINS disease expressing splicing variants that caused in-frame exon skipping. Despite the clear CADINS phenotype in heterozygous affected individuals, overexpression of the deletion constructs resulted in relatively moderate dominant-negative activity in the NF-κB assay. The relatively modest effect in the overexpression assay relative to the R30W CADINS variant could easily be explained by less expression in the assay, more robust effects in the context of physiological expression levels, or

alterations of other pathways that contribute to the clinical phenotypes (e.g., mTORC1 signaling[6]). Although splicing defects in other genes can lead to haploinsufficiency due to nonsense-mediated decay,[45] the extent to which in-frame splicing leads directly to altered protein function and disease is underappreciated. Although 9% of exons should be "in-frame" if skipped, genomic panels and traditional sequencing approaches treat splice variants as loss-of-function. Given no evidence of CARD11 haploinsufficiency to date, mere loss of expression of the mutated allele is likely not enough to cause disease. Our data demonstrate that splice variants should be evaluated for damaging effects on protein function and that SGE may be a useful tool for assessing the functional effects of splice variants.

Overall, we present an improved cloning-free SGE for use in diploid cells that coupled survival with drug selection to identify thousands of variants in *CARD11*, a clinically actionable gene. We demonstrate a high sensitivity and specificity for predicting pathogenicity and functionally classifying both variants previously found in patients with disease that decrease or increase *CARD11* function. Additionally, we identified a group of in-frame *CARD11* splicing defects that cause a dominant phenotype similar to other *CARD11* dominant-negative variants. The SGE functional data were immediately useful for diagnosing CADINS disease in two families with splice defects and five additional families with missense variants. It should be noted that in the absence of definitive clinical data (see Supplemental Note), variants that decrease *CARD11* function in our assay should be further tested to determine whether they exhibit dominant-negative activity or are solely loss-of-function. Finally, many other clinically relevant immune genes (*STAT3*,[46] *STAT1*,[47] and *NFKB2*,[48,49] among many others) can exhibit disease-associated variants that both decrease or increase protein function and will be high value targets for future SGE.

Data and Code Availability

The amplicon sequencing datasets generated in this study have been deposited on the Gene Expression Omnibus, record number GEO: GSE152129. The published article includes an explicit description of published analysis tools used to process and analyze the data. Any custom python scripts described in the Supplemental Material and Methods for routine analysis are available upon request.

Web Resources

GEO, https://www.ncbi.nlm.nih.gov/geo/
OMIM, https://www.omim.org/
RCSB Protein Data Bank, http://www.rcsb.org/pdb/home/home.do

References

1. Lek, M., Karczewski, K.J., Minikel, E.V., Samocha, K.E., Banks, E., Fennell, T., O'Donnell-Luria, A.H., Ware, J.S., Hill, A.J., Cummings, B.B., et al.; Exome Aggregation Consortium (2016). Analysis of protein-coding genetic variation in 60,706 humans. Nature *536*, 285–291.

2. Landrum, M.J., Lee, J.M., Riley, G.R., Jang, W., Rubinstein, W.S., Church, D.M., and Maglott, D.R. (2014). ClinVar: public archive of relationships among sequence variation and human phenotype. Nucleic Acids Res. *42*, D980–D985.

3. Richards, S., Aziz, N., Bale, S., Bick, D., Das, S., Gastier-Foster, J., Grody, W.W., Hegde, M., Lyon, E., Spector, E., et al.; ACMG Laboratory Quality Assurance Committee (2015). Standards and guidelines for the interpretation of sequence variants: a joint consensus recommendation of the American College of Medical Genetics and Genomics and the Association for Molecular Pathology. Genet. Med. *17*, 405–424.

4. Lu, H.Y., Bauman, B.M., Arjunaraja, S., Dorjbal, B., Milner, J.D., Snow, A.L., and Turvey, S.E. (2018). The CBM-opathies-A Rapidly Expanding Spectrum of Human Inborn Errors of Immunity Caused by Mutations in the CARD11-BCL10-MALT1 Complex. Front. Immunol. *9*, 2078.

5. Ma, C.A., Stinson, J.R., Zhang, Y., Abbott, J.K., Weinreich, M.A., Hauk, P.J., Reynolds, P.R., Lyons, J.J., Nelson, C.G., Ruffo, E., et al. (2017). Germline hypomorphic CARD11 mutations in severe atopic disease. Nat. Genet. *49*, 1192–1201.

6. Dorjbal, B., Stinson, J.R., Ma, C.A., Weinreich, M.A., Miraghazadeh, B., Hartberger, J.M., Frey-Jakobs, S., Weidinger, S., Moebus, L., Franke, A., et al. (2019). Hypomorphic caspase activation and recruitment domain 11 (CARD11) mutations associated with diverse immunologic phenotypes with or without atopic disease. J. Allergy Clin. Immunol. *143*, 1482–1495.

7. Greil, J., Rausch, T., Giese, T., Bandapalli, O.R., Daniel, V., Bekeredjian-Ding, I., Stütz, A.M., Drees, C., Roth, S., Ruland, J., et al. (2013). Whole-exome sequencing links caspase recruitment domain 11 (CARD11) inactivation to severe combined immunodeficiency. J. Allergy Clin. Immunol. *131*, 1376–1383.e3.

8. Stepensky, P., Keller, B., Buchta, M., Kienzler, A.K., Elpeleg, O., Somech, R., et al. (2013). Deficiency of caspase recruitment domain family, member 11 (CARD11), causes profound combined immunodeficiency in human subjects. J Allergy Clin Immunol *131*, 477–485.e1.

9. Fowler, D.M., Araya, C.L., Fleishman, S.J., Kellogg, E.H., Stephany, J.J., Baker, D., and Fields, S. (2010). High-resolution mapping of protein sequence-function relationships. Nat. Methods *7*, 741–746.

10. Brnich, S.E., Abou Tayoun, A.N., Couch, F.J., Cutting, G.R., Greenblatt, M.S., Heinen, C.D., Kanavy, D.M., Luo, X., McNulty, S.M., Starita, L.M., et al.; Clinical Genome Resource Sequence Variant Interpretation Working Group (2019). Recommendations for application of the functional evidence PS3/BS3 criterion using the ACMG/AMP sequence variant interpretation framework. Genome Med. *12*, 3. https://doi.org/10.1186/s13073-019-0690-2.

11. Gelman, H., Dines, J.N., Berg, J., Berger, A.H., Brnich, S., Hisama, F.M., James, R.G., Rubin, A.F., Shendure, J., Shirts, B., et al.; Brotman Baty Institute Mutational Scanning Working Group (2019). Recommendations for the collection and use of multiplexed functional data for clinical variant interpretation. Genome Med. *11*, 85.

12. Starita, L.M., Young, D.L., Islam, M., Kitzman, J.O., Gullingsrud, J., Hause, R.J., Fowler, D.M., Parvin, J.D., Shendure, J., and Fields, S. (2015). Massively Parallel Functional Analysis of BRCA1 RING Domain Variants. Genetics *200*, 413–422.

13. Mighell, T.L., Evans-Dutson, S., and O'Roak, B.J. (2018). A Saturation Mutagenesis Approach to Understanding PTEN Lipid Phosphatase Activity and Genotype-Phenotype Relationships. Am. J. Hum. Genet. *102*, 943–955.

14. Suiter, C.C., Moriyama, T., Matreyek, K.A., Yang, W., Scaletti, E.R., Nishii, R., Yang, W., Hoshitsuki, K., Singh, M., Trehan, A., et al. (2020). Massively parallel variant characterization identifies *NUDT15* alleles associated with thiopurine toxicity. Proc. Natl. Acad. Sci. USA *117*, 5394–5401.

15. Klein, J.C., Keith, A., Rice, S.J., Shepherd, C., Agarwal, V., Loughlin, J., and Shendure, J. (2019). Functional testing of thousands of osteoarthritis-associated variants for regulatory activity. Nat. Commun. *10*, 2434.

16. Matreyek, K.A., Starita, L.M., Stephany, J.J., Martin, B., Chiasson, M.A., Gray, V.E., Kircher, M., Khechaduri, A., Dines, J.N., Hause, R.J., et al. (2018). Multiplex assessment of protein variant abundance by massively parallel sequencing. Nat. Genet. *50*, 874–882.

17. Findlay, G.M., Daza, R.M., Martin, B., Zhang, M.D., Leith, A.P., Gasperini, M., Janizek, J.D., Huang, X., Starita, L.M., and Shendure, J. (2018). Accurate classification of BRCA1 variants with saturation genome editing. Nature *562*, 217–222.

18. Kotler, E., Shani, O., Goldfeld, G., Lotan-Pompan, M., Tarcic, O., Gershoni, A., Hopf, T.A., Marks, D.S., Oren, M., and Segal, E. (2018). A Systematic p53 Mutation Library Links Differential Functional Impact to Cancer Mutation Pattern and Evolutionary Conservation. Mol. Cell *71*, 178–190.e8.

19. Giacomelli, A.O., Yang, X., Lintner, R.E., McFarland, J.M., Duby, M., Kim, J., Howard, T.P., Takeda, D.Y., Ly, S.H., Kim, E., et al. (2018). Mutational processes shape the landscape of TP53 mutations in human cancer. Nat. Genet. *50*, 1381–1387.

20. Findlay, G.M., Boyle, E.A., Hause, R.J., Klein, J.C., and Shendure, J. (2014). Saturation editing of genomic regions by multiplex homology-directed repair. Nature *513*, 120–123.

21. Sanson, K.R., Hanna, R.E., Hegde, M., Donovan, K.F., Strand, C., Sullender, M.E., Vaimberg, E.W., Goodale, A., Root, D.E., Piccioni, F., and Doench, J.G. (2018). Optimized libraries for CRISPR-Cas9 genetic screens with multiple modalities. Nat. Commun. *9*, 5416.

22. Hung, K.L., Meitlis, I., Hale, M., Chen, C.-Y., Singh, S., Jackson, S.W., Miao, C.H., Khan, I.F., Rawlings, D.J., and James, R.G. (2018). Engineering Protein-Secreting Plasma Cells by Homology-Directed Repair in Primary Human B Cells. Mol. Ther. *26*, 456–467.

23. Richardson, C.D., Ray, G.J., DeWitt, M.A., Curie, G.L., and Corn, J.E. (2016). Enhancing homology-directed genome editing by catalytically active and inactive CRISPR-Cas9 using asymmetric donor DNA. Nat. Biotechnol. *34*, 339–344.

24. Rubin, A.F., Gelman, H., Lucas, N., Bajjalieh, S.M., Papenfuss, A.T., Speed, T.P., and Fowler, D.M. (2017). A statistical framework for analyzing deep mutational scanning data. Genome Biol. *18*, 150.

25. Pinard, A., Guey, S., Guo, D., Cecchi, A.C., Kharas, N., Wallace, S., Regalado, E.S., Hostetler, E.M., Sharrief, A.Z., Bergametti, F., et al. (2020). The pleiotropy associated with de novo variants in CHD4, CNOT3, and SETD5 extends to moyamoya angiopathy. Genet. Med. *22*, 427–431.

26. Pintilie, G.D., Zhang, J., Goddard, T.D., Chiu, W., and Gossard, D.C. (2010). Quantitative analysis of cryo-EM density map segmentation by watershed and scale-space filtering, and fitting of structures by alignment to regions. J. Struct. Biol. *170*, 427–438.

27. Schlauderer, F., Seeholzer, T., Desfosses, A., Gehring, T., Strauss, M., Hopfner, K.-P., Gutsche, I., Krappmann, D., and Lammens, K. (2018). Molecular architecture and regulation of BCL10-MALT1 filaments. Nat. Commun. *9*, 4041.

28. Webb, B., and Sali, A. (2014). Comparative Protein Structure Modeling Using MODELLER. Curr. Protoc. Bioinformatics *47*, 1–32.

29. Rawlings, D.J., Sommer, K., and Moreno-García, M.E. (2006). The CARMA1 signalosome links the signalling machinery of adaptive and innate immunity in lymphocytes. Nat. Rev. Immunol. *6*, 799–812.

30. Davis, R.E., Ngo, V.N., Lenz, G., Tolar, P., Young, R.M., Romesser, P.B., Kohlhammer, H., Lamy, L., Zhao, H., Yang, Y., et al. (2010). Chronic active B-cell-receptor signalling in diffuse large B-cell lymphoma. Nature *463*, 88–92.

31. Wilson, W.H., Young, R.M., Schmitz, R., Yang, Y., Pittaluga, S., Wright, G., Lih, C.-J., Williams, P.M., Shaffer, A.L., Gerecitano, J., et al. (2015). Targeting B cell receptor signaling with ibrutinib in diffuse large B cell lymphoma. Nat. Med. *21*, 922–926.

32. Lu, H.Y., Biggs, C.M., Blanchard-Rohner, G., Fung, S.-Y., Sharma, M., and Turvey, S.E. (2019). Germline CBM-opathies:

From immunodeficiency to atopy. J. Allergy Clin. Immunol. *143*, 1661–1673.

33. Kan, Y., Ruis, B., Takasugi, T., and Hendrickson, E.A. (2017). Mechanisms of precise genome editing using oligonucleotide donors. Genome Res. *27*, 1099–1111.

34. Chan, W., Schaffer, T.B., and Pomerantz, J.L. (2013). A quantitative signaling screen identifies CARD11 mutations in the CARD and LATCH domains that induce Bcl10 ubiquitination and human lymphoma cell survival. Mol. Cell. Biol. *33*, 429–443.

35. Kircher, M., Witten, D.M., Jain, P., O'Roak, B.J., Cooper, G.M., and Shendure, J. (2014). A general framework for estimating the relative pathogenicity of human genetic variants. Nat. Genet. *46*, 310–315.

36. Sun, S., Yang, F., Tan, G., Costanzo, M., Oughtred, R., Hirschman, J., Theesfeld, C.L., Bansal, P., Sahni, N., Yi, S., et al. (2016). An extended set of yeast-based functional assays accurately identifies human disease mutations. Genome Res. *26*, 670–680.

37. Dadi, H., Jones, T.A., Merico, D., Sharfe, N., Ovadia, A., Schejter, Y., Reid, B., Sun, M., Vong, L., Atkinson, A., et al. (2018). Combined immunodeficiency and atopy caused by a dominant negative mutation in caspase activation and recruitment domain family member 11 (CARD11). J. Allergy Clin. Immunol. *141*, 1818–1830.e2.

38. Qiao, Q., Yang, C., Zheng, C., Fontán, L., David, L., Yu, X., Bracken, C., Rosen, M., Melnick, A., Egelman, E.H., and Wu, H. (2013). Structural architecture of the CARMA1/Bcl10/MALT1 signalosome: nucleation-induced filamentous assembly. Mol. Cell *51*, 766–779.

39. Holliday, M.J., Witt, A., Rodríguez Gama, A., Walters, B.T., Arthur, C.P., Halfmann, R., Rohou, A., Dueber, E.C., and Fairbrother, W.J. (2019). Structures of autoinhibited and polymerized forms of CARD9 reveal mechanisms of CARD9 and CARD11 activation. Nat. Commun. *10*, 3070.

40. Li, S., Yang, X., Shao, J., and Shen, Y. (2012). Structural insights into the assembly of CARMA1 and BCL10. PLoS ONE *7*, e42775.

41. Hara, H., Wada, T., Bakal, C., Kozieradzki, I., Suzuki, S., Suzuki, N., Nghiem, M., Griffiths, E.K., Krawczyk, C., Bauer, B., et al.

(2003). The MAGUK family protein CARD11 is essential for lymphocyte activation. Immunity *18*, 763–775.

42. Bedsaul, J.R., Carter, N.M., Deibel, K.E., Hutcherson, S.M., Jones, T.A., Wang, Z., Yang, C., Yang, Y.-K., and Pomerantz, J.L. (2018). Mechanisms of Regulated and Dysregulated CARD11 Signaling in Adaptive Immunity and Disease. Front. Immunol. *9*, 2105.

43. David, L., Li, Y., Ma, J., Garner, E., Zhang, X., and Wu, H. (2018). Assembly mechanism of the CARMA1-BCL10-MALT1-TRAF6 signalosome. Proc. Natl. Acad. Sci. USA *115*, 1499–1504.

44. McAllister-Lucas, L.M., Inohara, N., Lucas, P.C., Ruland, J., Benito, A., Li, Q., Chen, S., Chen, F.F., Yamaoka, S., Verma, I.M., et al. (2001). Bimp1, a MAGUK family memberlinking protein kinase C activation to Bcl10-mediated NF-kappaB induction. J. Biol. Chem. *276*, 30589–30597.

45. Kurosaki, T., Popp, M.W., and Maquat, L.E. (2019). Quality and quantity control of gene expression by nonsense-mediated mRNA decay. Nat. Rev. Mol. Cell Biol. *20*, 406–420.

46. Vogel, T.P., Milner, J.D., and Cooper, M.A. (2015). The Ying and Yang of STAT3 in Human Disease. J. Clin. Immunol. *35*, 615–623.

47. Olbrich, P., and Freeman, A.F. (2018). STAT1 and STAT3 mutations: important lessons for clinical immunologists. Expert Rev. Clin. Immunol. *14*, 1029–1041.

48. Slade, C.A., McLean, C., Scerri, T., Giang, T.B., Megaloudis, S., Strathmore, A., Tempany, J.C., Nicholls, K., D'Arcy, C., Bahlo, M., et al. (2019). Fatal Enteroviral Encephalitis in a Patient with Common Variable Immunodeficiency Harbouring a Novel Mutation in NFKB2. J. Clin. Immunol. *39*, 324–335.

49. Chen, K., Coonrod, E.M., Kumánovics, A., Franks, Z.F., Durtschi, J.D., Margraf, R.L., Wu, W., Heikal, N.M., Augustine, N.H., Ridge, P.G., et al. (2013). Germline mutations in NFKB2 implicate the noncanonical NF-κB pathway in the pathogenesis of common variable immunodeficiency. Am. J. Hum. Genet. *93*, 812–824.